PHYSICAL REVIEW C **96**, 014321 (2017)

First-excited state g factor of ^{136}Te by the recoil in vacuum method

A. E. Stuchbery,[1,*] J. M. Allmond,[2] M. Danchev,[3,4] C. Baktash,[2] C. R. Bingham,[2,4] A. Galindo-Uribarri,[2,4] D. C. Radford,[2] N. J. Stone,[4,5] and C.-H. Yu[2]

[1]*Department of Nuclear Physics, Research School of Physics and Engineering, Australian National University, Canberra ACT 2601, Australia*
[2]*Physics Division, Oak Ridge National Laboratory, Oak Ridge, Tennessee 37831, USA*
[3]*Faculty of Physics, St. Kliment Ohridski University of Sofia, 1164 Sofia, Bulgaria*
[4]*Department of Physics and Astronomy, University of Tennessee, Knoxville, Tennessee 37996, USA*
[5]*Department of Physics, Oxford University, Oxford OX1 3PU, United Kingdom*

(Received 1 June 2017; published 27 July 2017)

The g factor of the first 2^+ state of radioactive ^{136}Te with two valence protons and two valence neutrons beyond double-magic ^{132}Sn has been measured by the recoil in vacuum (RIV) method. The lifetime of this state is an order of magnitude longer than the lifetimes of excited states recently measured by the RIV method in Sn and Te isotopes, requiring a new evaluation of the free-ion hyperfine interactions and methodology used to determine the g factor. The calibration data are reported and the analysis procedures are described in detail. The resultant g factor has a similar magnitude to the g factors of other nuclei with an equal number of valence protons and neutrons in the major shell. However, an unexpected trend is found in the g factors of the $N = 84$ isotones, which decrease from ^{136}Te to ^{144}Nd. Shell model calculations with interactions derived from the CD Bonn potential show good agreement with the g factors and $E2$ transition rates of 2^+ states around ^{132}Sn, confirming earlier indications that ^{132}Sn is a good doubly magic core.

DOI: 10.1103/PhysRevC.96.014321

I. INTRODUCTION

The properties of nuclei with a few nucleons beyond neutron-rich doubly magic ^{132}Sn are of considerable current interest. The excitation energies, transition rates, and static moments are sensitive to shell structure, the strength of the proton-neutron interactions, and to developing collectivity [1–10]. Following the observation of an anomalously low $B(E2; 0_1^+ \rightarrow 2_1^+)$ by Radford *et al.* [11], the case of ^{136}Te, with two protons and two neutrons outside the ^{132}Sn core, has been the subject of many theoretical studies, with widely varying predictions of the electromagnetic properties of the low-excitation states [1–5,9,10]. In particular, the various calculations make disparate predictions of the g factor of the first-excited state in ^{136}Te; the calculations disagree on both the sign and magnitude of the g factor. This paper concerns a measurement of the magnitude of this g factor by the recoil in vacuum (RIV) method.

The RIV technique has proved to be a powerful method to measure the g factors of excited states of neutron-rich nuclei produced as radioactive beams, particularly in the tin and tellurium isotopes near the neutron-rich doubly magic nuclide ^{132}Sn [12–16]. One of the method's advantages is that the g factor of the 2_1^+ state can be measured simultaneously with the $B(E2; 0^+ \rightarrow 2^+)$ and $Q(2^+)$ [14–18]. Although the RIV method gives only the magnitude of the g factor, it has proven to give it more precisely [12,13,15] than the transient-field method [19,20] in the case of radioactive beam measurements where statistical precision is limited. The advantage of the transient-field method, however, is that it can determine the sign.

To date, the RIV method has been applied to stable and radioactive beams of the Sn and Te isotopes to determine the g factors of states with mean lifetimes in the range from $\tau \sim 0.5$ ps for ^{112,114,116}Sn [16] to $\tau \sim 2.5$ ps for ^{132}Te [12,13] and ^{128}Sn [15]. In these measurements the RIV interaction could be calibrated empirically [13] or semiempirically [12–15,15,16], with similar results [12,13,21]. The key ingredients determining the hyperfine interaction calibration and its reliability in the previous work were: (i) the independently measured $g(2_1^+)$ of ^{130}Te with $\tau = 3.4$ ps, which serves as the primary reference value for the hyperfine interaction calibration, (ii) the evidence that the hyperfine interaction is effectively static during the lifetime of states with $\tau \lesssim 3$ ps, and (iii) that the vacuum attenuation coefficients approach unity as either g or τ approaches zero. Thus the measurements to date are anchored between the experimental attenuation coefficients for ^{130}Te and unity, with a constrained interpolation. Additional data on ^{126}Te ($\tau = 6.5$ ps) and ^{122}Te ($\tau = 10.8$ ps) have served to guide the empirical parametrization of the effect of RIV on the observed angular correlations and give insights into the physics of the free-ion hyperfine interactions on which the RIV method depends [12,13,21].

The challenge addressed in the present work is that the lifetime of the 2_1^+ state in ^{136}Te is an order of magnitude longer than the lifetimes of the states to which the RIV method has been applied in the ^{132}Sn region. While the result for $g(2_1^+)$ in ^{136}Te has been published in Letter form [18], along with $Q(2_1^+)$ and $B(E2)$ values, the present paper reports the calibration data on which the g-factor measurement depends, and discusses in detail the procedures developed for the analysis of the calibration data and the g-factor measurement.

The paper is arranged as follows. The experiment is described in Sec. II. The following section presents the results and gives details of the analysis procedures. The angular

*Corresponding author: andrew.stuchbery@anu.edu.au

 ©2017 American Physical Society

correlations are presented first and analyzed to obtain attenuation coefficients for the series of stable-beam calibration measurements performed. After a brief review of the RIV formalism, the procedure is developed to relate the attenuation coefficients to the g factor. This procedure is then used to obtain the g factors of ^{136}Te and ^{126}Te; the stable ^{126}Te case serves as a check on the methodology. The Discussion is divided into two sections. In Sec. IV, the analysis procedures are discussed in detail and the impact of these procedures on the extracted g factor is evaluated. This section concludes with a review of the status of atomic physics calculations that seek to determine the RIV calibration from first principles. In Sec. V, the nuclear structure implications of the g-factor measurement are discussed, first in terms of the g-factor systematics in the major shell. Then follows a comparison of experimental results with shell model calculations. An overview of theoretical and experimental g factors and $B(E2)$ values is presented for nuclei with a few valence nucleons outside ^{132}Sn.

II. EXPERIMENT

The principle on which the RIV method is based is that when a free ion moves through vacuum, the hyperfine interaction couples the atomic spin $\boldsymbol{J}$ to the nuclear spin $\boldsymbol{I}$ and together they precess about the total spin $\boldsymbol{F} = \boldsymbol{I} + \boldsymbol{J}$. The precession frequency depends on the strength of the hyperfine interaction which in turn depends on the magnitude of the nuclear g factor. To measure the g factor, the nuclear state of interest is excited by a suitable reaction and then allowed to recoil into vacuum, typically as a highly charged ion. The effect of the hyperfine interaction is observed via the perturbation of the angular correlation/distribution of the γ rays de-exciting the state. Thus, in general terms, considering the Coulomb excitation of radioactive ion beams, the $B(E2)$ is determined from the total γ-ray intensity whereas the g factor is determined from its angular distribution.

In the presence of vacuum deorientation, the particle-γ angular correlation after Coulomb excitation takes the form (see Refs. [22–24] and references therein)

$$W(\theta_p,\theta_\gamma,\Delta\phi) = \sum_{kq} B_{kq}(\theta_p) Q_k G_k F_k D^{k*}_{q0}(\Delta\phi,\theta_\gamma,0), \quad (1)$$

where (θ_p,ϕ_p) and $(\theta_\gamma,\phi_\gamma)$ are the spherical polar angles corresponding to particle and γ-ray detection, respectively, with the z axis along the beam direction, and $\Delta\phi = \phi_\gamma - \phi_p$. The attenuation coefficients, G_k, specify the vacuum deorientation effect; $B_{kq}(\theta_p)$ is the statistical tensor, which defines the spin alignment of the initial state. F_k represents the usual F coefficient for the γ-ray transition, Q_k is the attenuation factor for the finite size of the γ-ray detector, and $D^{k*}_{q0}(\Delta\phi,\theta_\gamma,0)$ is the rotation matrix. In the applications of interest $k = 0,2,4$.

A radioactive ion beam of ^{136}Te at an energy of 410 MeV was Coulomb excited on a 1.5-mg/cm^2 titanium target, 81% ^{50}Ti [18]. The measurement was performed at the Holifield Radioactive Ion Beam Facility (HRIBF) of Oak Ridge National Laboratory (ORNL). The experimental setup included a HPGe Clover array, CLARION [25], a 2π CsI array, BareBall [26], and a Bragg-Curve detector. CLARION had four detectors at $\theta_\gamma = 90^\circ$ with $\phi_\gamma = 51.4^\circ$, 102.9°, 154.3°, and 257.2°; four detectors at $\theta_\gamma = 132^\circ$ with $\phi_\gamma = 26^\circ$, 154°, 206°, and 334°; and two detectors at $\theta_\gamma = 154^\circ$ with $\phi_\gamma = 90^\circ$, and 270°. The beam direction defines $\theta = 0^\circ$ and $\phi = 0^\circ$ is vertically upwards.

TABLE I. Experimental details. The same ^{50}Ti target was used for all measurements. v/c is the average velocity with which excited beam ions enter vacuum as determined from the observed Doppler shift (uncertainties are ±0.03%). Measurements with the same run number were performed together, with the same detector arrangement.

Beam	E_{beam} (MeV)	Run	v/c (%)		
			Ring 2 14–28°	Ring 3 28–44°	Ring 4 44–60°
^{136}Te	410	I	3.59	4.71	5.82
^{126}Te	390	I	3.47	4.62	5.82
^{122}Te	378	II	3.32	4.54	5.73
^{124}Te	385	II	3.41	4.57	5.75
^{125}Te	390	II	3.53	4.65	5.79
^{126}Te	390	II	3.49	4.64	5.81
^{130}Te	400	II	3.54	4.65	5.84

Coulomb-excitation cross sections and particle-γ angular correlations were measured at four different recoiling target angles using rings 1 through 4 of BareBall, covering $\theta_{\text{lab}} = 7^\circ$–$60^\circ$ or $\theta_{\text{c.m.}} = 166^\circ$–$60^\circ$. Measurements on stable ^{126}Te were also performed under the same conditions during the same beam time, designated Run I in Table I. Data from ring 1 were useful for determining $B(E2)$ values and $Q(2^+_1)$, but were of insufficient statistical precision to contribute to the g-factor measurement. The present work therefore focuses on data collected in rings 2–4, corresponding to $\theta_{\text{lab}} = 14^\circ$–$60^\circ$. BareBall has ten azimuthal segments in ring 2, and 12 azimuthal segments in rings 3 and 4.

To calibrate the RIV interaction, additional experiments on the stable Te beams listed in Table I were performed in a separate beam time, designated Run II. In these stable-beam measurements the same apparatus was used but the number of Clover detectors in CLARION was reduced to three detectors in the $\theta_\gamma = 90^\circ$ ring (at $\phi_\gamma = 102.9^\circ$, 154.3°, and 205.8°) and three detectors in the $\theta_\gamma = 132^\circ$ ring (at $\phi_\gamma = 154^\circ$, 206°, and 334°).

The v/c exit-velocity values of the excited ions reported in Table I were measured directly from the observed Doppler-shifted γ-ray energies on a per BareBall ring basis. These values were confirmed by comparing them with expectations based on kinematic calculations and experimental energy-loss measurements with the Bragg-curve detector.

III. RESULTS AND ANALYSIS

A. Angular correlations

Examples of γ-ray spectra are shown in Fig. 1. The four transitions of interest between 408 and 463 keV in ^{125}Te correspond to decays from the $3/2^+$ and $5/2^+$ states at 444 and 463 keV, respectively, to the $1/2^+$ ground state and $3/2^+$ state

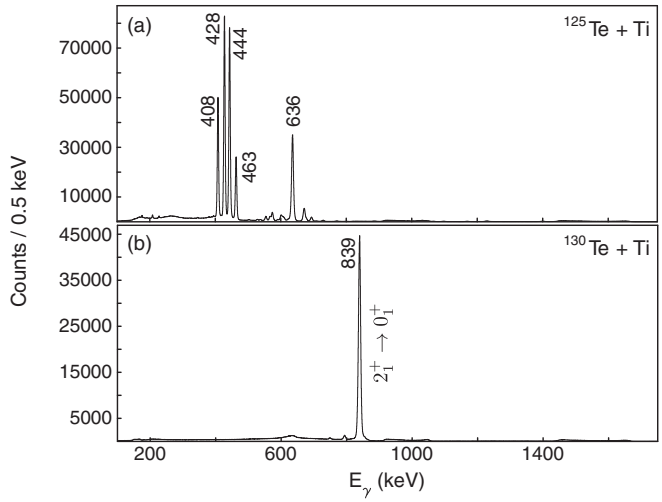

FIG. 1. Examples of γ-ray spectra in coincidence with Ti ions detected in rings 2, 3, and 4 of BareBall from (a) 390 MeV ^{125}Te and (b) 400 MeV ^{130}Te.

at 35 keV. The 636-keV line between the 671-keV $5/2^+$ and 35-keV $3/2^+$ states bypasses the states of interest. As evident in Fig. 1, there is weak feeding from higher-excited states into the states of interest, particularly for ^{125}Te; this feeding was included in the evaluation of the angular correlations, however the difference between including and neglecting the feeding was negligible.

Particle-γ angular correlations for ^{122}Te and ^{125}Te are presented in Figs. 2 and 3. In these figures, the angular correlations are normalized as follows: If the coincidence count rate in a chosen pair of particle and γ-ray detectors, $N(\theta_p,\theta_\gamma,\phi_\gamma - \phi_{p_i})$, is normalized to the coincidence rate summed over all of the particle detectors in the particular BareBall ring, the

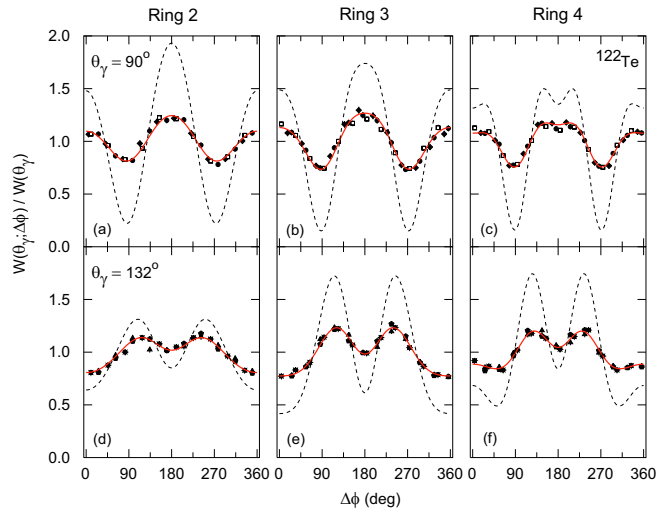

FIG. 2. Angular correlations of ^{122}Te excited on Ti. (a)–(c) correspond to $\theta_\gamma = 90^\circ$, (d)–(f) to $\theta_\gamma = 132^\circ$. The unperturbed correlations are indicated by the dotted curves; solid red lines show the fit to the attenuated angular correlations. See text for details of the normalization procedure.

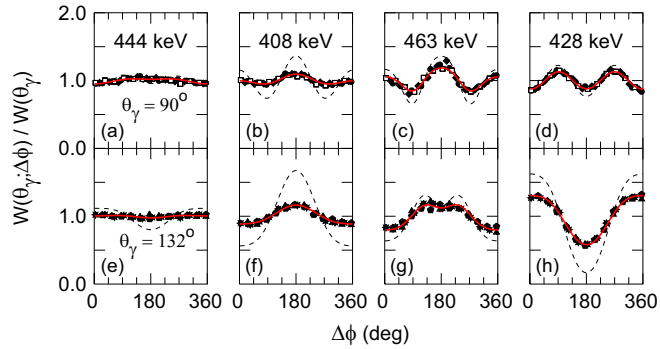

FIG. 3. Angular correlations of ^{125}Te excited on Ti with Ti recoils detected in BareBall ring 3. (a)–(d) correspond to $\theta_\gamma = 90^\circ$, (e)–(h) to $\theta_\gamma = 132^\circ$. The unperturbed correlations are indicated by the dotted curves; solid red lines show the fit to the attenuated angular correlations. The transitions are 444 keV ($3/2_2^+ \rightarrow 1/2_1^+$), 408 keV ($3/2_2^+ \rightarrow 3/2_1^+$), 463 keV ($5/2_1^+ \rightarrow 1/2_1^+$), and 428 keV ($5/2_1^+ \rightarrow 3/2_1^+$). See text for details of the normalization procedure.

unperturbed angular correlations can be calculated with no free parameters. In other words, this normalization procedure factors out the γ-ray detection efficiency, giving

$$\frac{N(\theta_p,\theta_\gamma,\phi_\gamma - \phi_{p_i})}{\sum_{i=1}^{N_R} N(\theta_p,\theta_\gamma,\phi_\gamma - \phi_{p_i})/N_R} = \frac{W(\theta_p,\theta_\gamma,\phi_\gamma - \phi_{p_i})}{W(\theta_p,\theta_\gamma)}, \quad (2)$$

where N_R is the number of detectors (i.e., azimuthal segments) in the BareBall ring and $W(\theta_p,\theta_\gamma)$ is given by Eq. (1) with $q \equiv 0$. (The subscript i is included in the designation of the particle detection angle ϕ_{p_i} in order to designate the sum over segments in the BareBall ring. The relative efficiencies of the BareBall segments are nominally identical; this assumption can be checked against the observed Rutherford scattering rates.) By this procedure, the only free parameters required to fit the perturbed angular correlations are the vacuum attenuation factors, G_2 and G_4.

The ^{136}Te angular correlation data from BareBall rings 3 and 4 are represented in Fig. 4; these data largely determine the g factor, whereas ring 2 contributes little to the g-factor measurement. Because the statistics of this radioactive beam measurement are low and distributed over more than 300 individual particle-γ combinations, it is difficult to judge the shape of the angular correlation and the overall statistical quality of the angular correlation measurement visually from a plot showing the individual data points. For presentation, therefore, the experimental data have been combined to produce six or seven data points in the interval $0 \leqslant \Delta\phi \leqslant 180^\circ$ for each Clarion and BareBall ring. (Note that these combined data were not used in the g-factor analysis.) It is clear from Fig. 4 that the $\theta_\gamma = 90^\circ$ data are most sensitive to the magnitude of the vacuum deorientation, and hence to the g factor, followed by the $\theta_\gamma = 132^\circ$ data and then the $\theta_\gamma = 154^\circ$ data.

B. Measured attenuation coefficients G_k

Table I indicates that the recoil velocity of the Te ions varies strongly with the scattering angle, and hence the BareBall

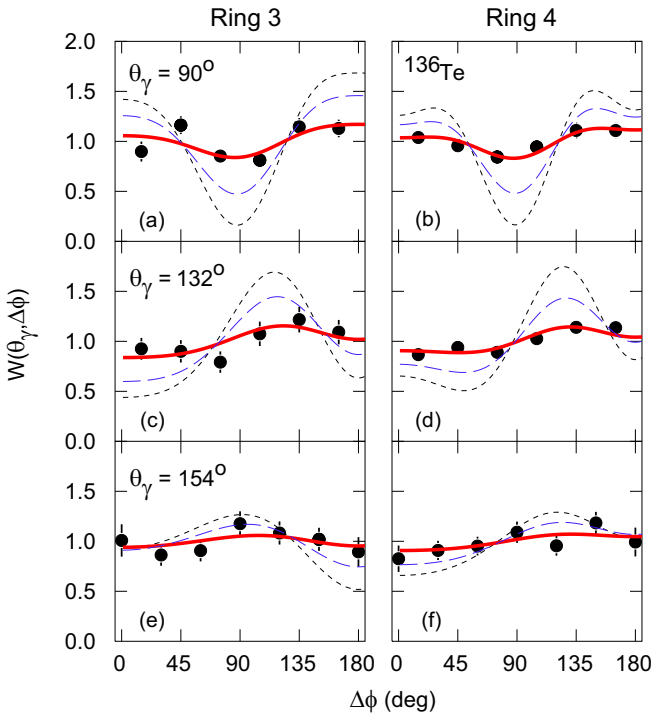

FIG. 4. Angular correlations of ^{136}Te excited on Ti. (a), (b) correspond to $\theta_\gamma = 90^\circ$, (c), (d) to $\theta_\gamma = 132^\circ$, and (e), (f) to $\theta_\gamma = 154^\circ$. To give a visual representation of the overall statistical quality of the angular correlation data, individual data points have been combined and projected onto the interval $0 \leqslant \Delta\phi \leqslant 180^\circ$. The red solid line indicates the best fit to the data (not combined). The black dotted line indicates the unperturbed angular correlation and the blue dashed line indicates the angular correlation that would be associated with $g = 0.1$.

ring number. There is a consequent variation in the average charge-state of the ions and hence of the strength of the hyperfine interactions. A separate calibration of the hyperfine interaction is therefore needed for each BareBall ring. There are small variations in recoil velocity from isotope to isotope, but as discussed below (Sec. IV), these have consequences well below the precision of the g-factor measurements and can be ignored in the present analysis.

Table II gives the measured attenuation coefficients G_2 and G_4 for each BareBall ring (combining data for $\theta_\gamma = 90^\circ$ and $\theta_\gamma = 132^\circ$) and for the series of calibration measurements on stable Te isotopes (Run II), along with the previously determined g factors and lifetimes.

C. RIV formalism

Before relating the measured attenuation coefficients, G_k, to the g factors, it is useful to review the fundamental relationship between them that applies in the simplest case where there is a single atomic state that persists throughout the lifetime of the nuclear level of interest.

The time-dependent attenuation coefficient for an electronic configuration of spin J, which produces an effective magnetic field B at the nucleus, is given by

$$G_k(t) = \sum_{F,F'} C_{IJ}^{FF'}(k)\cos(\omega_{FF'}t), \tag{3}$$

where

$$\omega_{FF'} = g\frac{\mu_N}{\hbar}B\frac{(F(F+1) - F'(F'+1))}{2J} \tag{4}$$

and

$$C_{IJ}^{FF'}(k) = \frac{(2F+1)(2F'+1)}{2J+1}\begin{Bmatrix} F & F' & k \\ I & I & J \end{Bmatrix}^2. \tag{5}$$

Note that the attenuation coefficients G_2 and G_4 differ only through the k value in the $6J$ symbol in Eq. (5). However, for the same atomic configuration with spin J, the G_k are different for different nuclear angular momenta, I, which also changes the range of values of the total angular momentum, F, in the above formulas.

In the experiments performed here, the Te ions emerge from the Ti target with a distribution of charge states and with the atomic electrons distributed in many excited atomic states. Consequently, there is a superposition of many hyperfine frequencies that gives a quasi-exponential time dependence to the vacuum attenuation factors, $G_k(t)$. Thus the alignment of the nuclear state, and hence the anisotropy of the γ-ray angular correlation, decreases approximately exponentially with time at a rate that depends on the magnitude of the nuclear g factor. More detailed descriptions, and examples which illustrate the emergence of a quasiexponential time dependence for $G_k(t)$, have been given in Refs. [13,35].

TABLE II. Excited state g factors, lifetimes and time-integrated vacuum attenuation coefficients.

Nuclide	I^π	E_x (keV)	g[a]	τ[b] (ps)	Ring 2		Ring 3		Ring 4	
					G_2	G_4	G_2	G_4	G_2	G_4
^{122}Te	2^+	564	0.353(14)	10.76(7)	0.503(24)	0.319(15)	0.410(10)	0.284(7)	0.338(9)	0.243(8)
^{124}Te	2^+	603	0.326(18)	8.95(14)	0.592(41)	0.363(27)	0.513(18)	0.324(12)	0.402(15)	0.286(13)
^{126}Te	2^+	666	0.339(13)	6.52(14)	0.693(50)	0.463(32)	0.603(22)	0.409(15)	0.520(18)	0.332(17)
^{130}Te	2^+	839	0.351(18)	3.32(7)	0.811(54)	0.669(35)	0.694(25)	0.609(19)	0.604(23)	0.535(26)
^{125}Te	$3/2^+$	444	0.59(5)	27.6(9)	0.252(15)	0	0.202(7)	0	0.172(6)	0
^{125}Te	$5/2^+$	463	0.207(22)	19.1(7)	0.638(35)	0.465(49)	0.533(4)	0.409(26)	0.454(3)	0.336(3)

[a] g factors from Refs. [27–29].
[b] Lifetimes from Nuclear Data Sheets [30–34].

D. Calibration: Relating G_k to g factor

Equation (5) indicates that G_2 and G_4 are intimately related to each other, although in the case of a complex superposition of static and time-varying hyperfine interactions, that relationship is not readily calculated from first principles. As evident from the results in Table II, experimental G_2 and G_4 values can be determined independently from fits to angular correlation data. It is advantageous to explore the empirical relationship between G_2 and G_4 from the stable-beam calibration data with a view to constraining it before fitting the much lower statistics radioactive beam data for ^{136}Te.

We begin with the fluctuating-field model of Abragam and Pound [36] for pure magnetic interactions, which does specify a simple relationship between G_2 and G_4, namely,

$$G_4 = \frac{0.3G_2}{1 - 0.7G_2}. \tag{6}$$

To parametrize the data we generalize this form as

$$G_4 = \frac{aG_2^p}{1 - (1-a)G_2^p}, \tag{7}$$

which has the correct limits that $G_4 \to 0$ as $G_2 \to 0$ and $G_4 \to 1$ as $G_2 \to 1$.

The experimental data for ^{122,124,126,130}Te are displayed in Fig. 5, along with fits to Eq. (7). For comparison, the Abragam-Pound expression, Eq. (6), is shown, along with the relationship between G_2 and G_4 implied by the empirical static model used in recent work to obtain g factors in ^{132,134}Te [13,14]. The parameters resulting from the fits are included in Table III.

The approach to relate the observed attenuation coefficients to the g factor, i.e., to calibrate the hyperfine interaction, in the present work is largely empirical, as described in Ref. [13]. The time-dependent attenuation coefficients are assumed to decay exponentially with time to a hard core value α_k at the limit of long times

$$G_k(t) = \alpha_k + (1 - \alpha_k)e^{-\Gamma_k t}. \tag{8}$$

The experiments considered here determine the time-integral attenuation factors

$$G_k^\infty(\tau) = \int_0^\infty G_k(t)\mathrm{e}^{-t/\tau}\mathrm{d}t/\tau, \tag{9}$$

where τ is the mean life of the nuclear state. Thus the integral attenuation coefficients have the form

$$G_k^\infty(\tau) = \alpha_k + (1 - \alpha_k)\frac{1}{1 + |\Gamma_k|\tau}. \tag{10}$$

TABLE III. Parameters a and p of G_4 versus G_2 fits, Eq. (7), and parameters of G_k versus $g^2\tau$ fits, Eq. (10), for each BareBall ring.

Ring	a	p	α_2	C_2	α_4	C_4
2	0.23	0.60	0.16(2)	1.10(7)	0.09(1)	0.50(3)
3	0.43	0.86	0.14(1)	0.71(3)	0.08(1)	0.37(2)
4	0.48	0.86	0.13(1)	0.49(2)	0.09(1)	0.30(2)

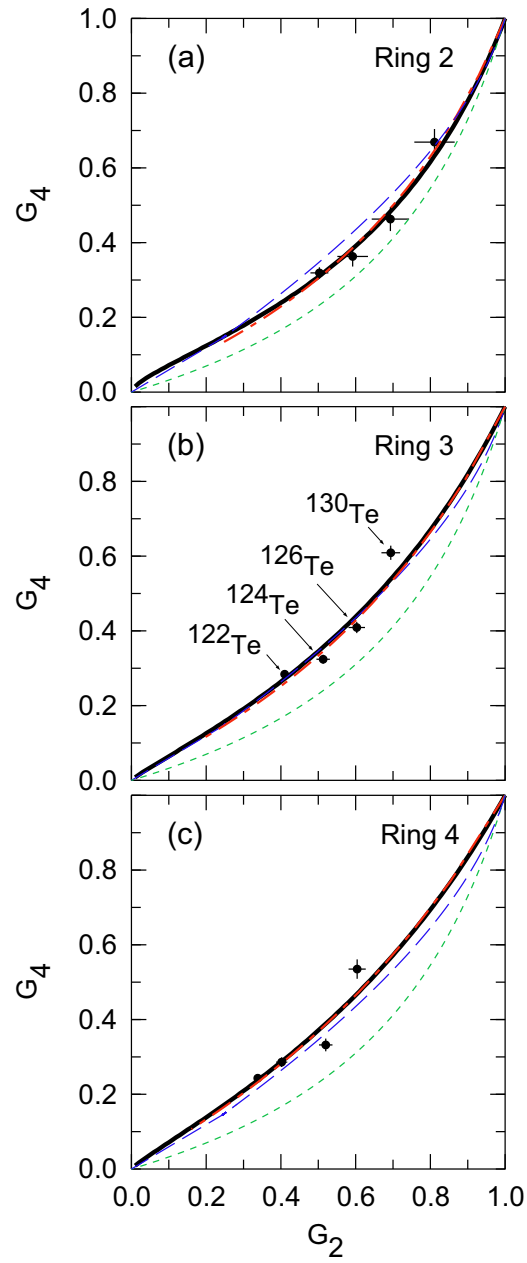

FIG. 5. Experimental data and G_4 parametrized as a function of G_2 for each BareBall ring: (a) ring 2, (b) ring 3, and (c) ring 4. Fits to Eq. (7) are shown as the black solid line. The parametrizations of G_k versus $g^2\tau$ used in the g-factor analysis give the red dot-dashed lines, which are almost indistinguishable from the solid black lines. The static model used previously to analyze RIV data on Sn and Te isotopes [14–16] is shown for reference (blue dashed line), as is the Abragam-Pound formula, Eq. (6), (green dotted line).

The dependence on the g factor is given by

$$\Gamma_k = |g^n|/C_k, \tag{11}$$

where C_k is the parameter that determines the strength of the interaction, and hence deorientation. The static limit (no atomic transitions) corresponds to $n = 1$ [13] whereas the fluctuating limit (continuous atomic transitions) corresponds

to $n = 2$ [36]. The parameters C_2, C_4, α_2, α_4, and n were determined based on experimental data for the excited states with known g factors and level lifetimes in the Te isotopes, as listed in Table II. On the one hand, the relationship between G_2 and G_4 is constrained by the data on the even isotopes, as presented in Fig. 5, while on the other, the ^{125}Te data are particularly important to determine the value of n and to set the value of α_k. More specifically, the $3/2^+$, 444-keV state in ^{125}Te, with mean life $\tau = 27.6$ ps and g factor $g = +0.59(5)$ [27–29], allows calibration of the RIV interaction out to the necessary lifetime and determines the hard core, at least for $k = 2$. The $5/2^+$ 463-keV state in ^{125}Te, with $\tau = 19.1$ ps and $g = +0.207(22)$ [27–29], has nearly the same $g\tau$ value as the 2_1^+ state in ^{122}Te ($\tau = 10.8$ ps, $g = +0.353(14)$ [27]), but as the two levels have very different g factors and lifetimes, the value of n can be determined. In fact it can be seen by inspection of the very different G_k values for these two states, shown in first and last rows of Table II, that $n \neq 1$.

Fits to the data in Table II were performed with n as a parameter, giving for rings 2–4, $n = 2.3^{+0.2}_{-0.3}$, $n = 2.2^{+0.4}_{-0.4}$, and $n = 2.1^{+0.4}_{-0.1}$, respectively, in all cases consistent with $n = 2$. As the difference between the inferred g factor for $n = 2.2$ and $n = 2$ is negligible, and as there is a precedent for $n = 2$ in the literature (see, e.g., [36–38]), $n = 2$ was adopted for subsequent analysis. The parameters for $n = 2$ are given in Table III. The resulting calibration curves are shown in Fig. 6, along with the experimental data and results of the ^{136}Te g-factor analysis.

E. g-factor results

The g factor of ^{136}Te was determined by fitting the angular correlation data (cf. Fig. 4) using Eq. (1) with the G_k coefficients related to $g^2\tau$ through Eq. (10) and the parameters for each BareBall ring as given in Table III. The result of the fit to determine $g^2\tau$ for ^{136}Te is indicated in Fig. 6. A g factor of $(+)0.34^{+0.08}_{-0.06}$ was then determined using $\tau = 27.5(23)$ ps from the simultaneous $B(E2)$ measurement [18]. The sign $(+)$ is tentatively set by systematics, and on the basis that no standard theory can predict a negative g factor of the observed magnitude. Consistent g factors were obtained from an analysis of the data for individual particle and γ-ray detector rings, albeit with larger statistical uncertainties. For example analysis of data for BareBall rings 2, 3, and 4 individually gave $g = 0.39^{+0.61}_{-0.13}$, $g = 0.37^{+0.16}_{-0.08}$, and $g = 0.30^{+0.09}_{-0.05}$, respectively.

The g factor of the first-excited state of ^{126}Te was determined by the same procedures from the ^{126}Te data taken during Run I. The result is $g(2^+) = 0.318(10)$, including statistical errors and the uncertainty in the lifetime, but no uncertainty in the parametrization of G_k versus $g^2\tau$. The adopted experimental value of the g factor is $g = +0.339(13)$ [27]. The difference between the adopted and extracted g factors, 0.021 ± 0.016, gives an indication of the uncertainty in the RIV calibration procedure. By adopting a calibration that excludes the ^{125}Te $3/2^+$ state, which in effect gives a better interpolation of the G_k coefficients in the relevant range (see Fig. 6) yields $g(2^+) = 0.332(9)$—in excellent agreement with the adopted g factor. This agreement also demonstrates that RIV experiments performed some time apart yield consistent results.

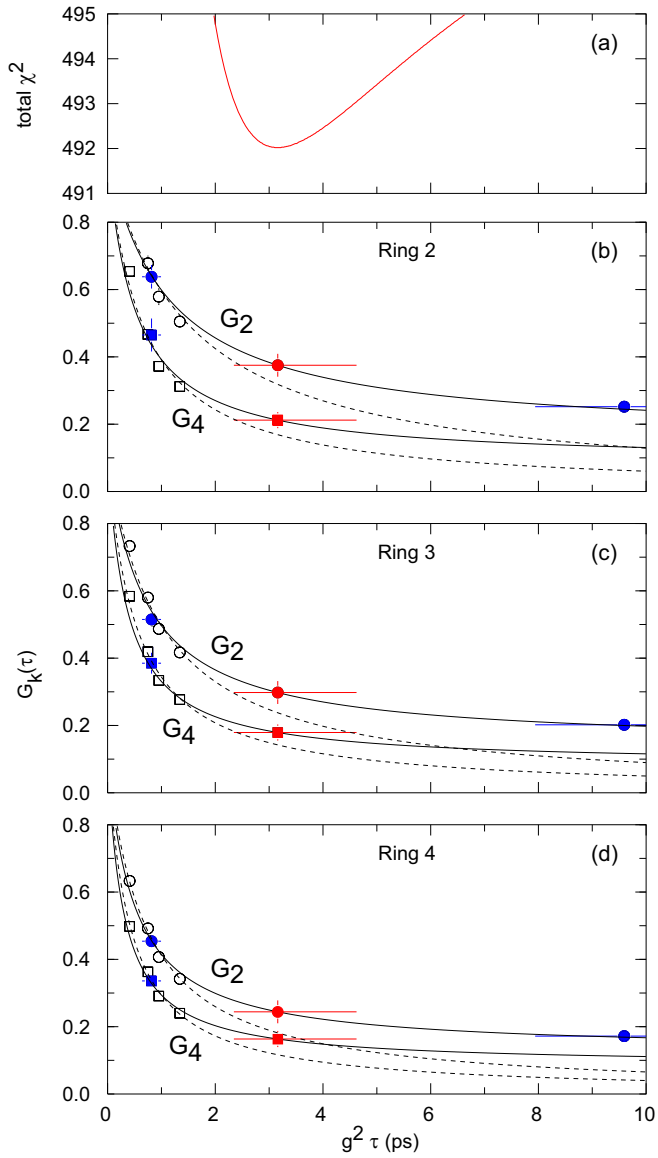

FIG. 6. (a) Total χ^2 versus $g^2\tau$. (b)–(d) G_k versus $g^2\tau$ calibration curves (solid lines) for BareBall rings 2–4. The best fit $g^2\tau$ value for ^{136}Te, and its uncertainty, is projected onto the curves (red filled). Also shown are the calibration data for the stable Te isotopes that define the G_k curves [13]. Results for ^{125}Te are blue filled. Note that there is no G_4 term for $I = 3/2$ states and that the differences in G_k values for $I = 3/2,2,5/2$ are negligible within the experimental uncertainty (Sec. IV A). The dotted lines indicate the calibration curves that result if the ^{125}Te $3/2^+$ state (extreme right data point) is ignored, which effectively sets the hard core parameter $\alpha_k = 0$.

IV. DISCUSSION OF ANALYSIS PROCEDURES

The adopted g factor of ^{136}Te results from a state of the art analysis procedure subject to the limitations of the current knowledge of the RIV interaction. It is useful to evaluate the sensitivity of the extracted g factor to the analysis procedures and approximations. Here we examine first the statement above that the difference between the attenuation coefficients for nuclear spins $I = 3/2, 2$, and $5/2$ can be neglected. Second, we

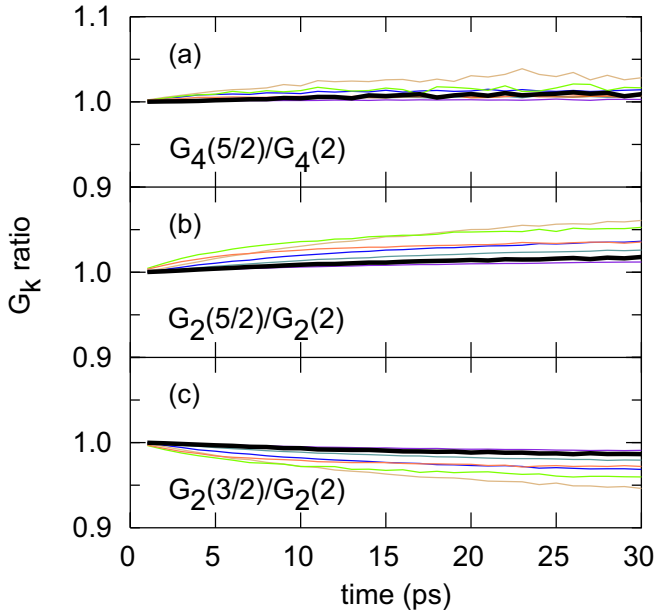

FIG. 7. Toy model Monte Carlo calculations of (a) $G_4(I = 5/2)/G_4(I = 2)$, (b) $G_2(I = 5/2)/G_2(I = 2)$, and (c) $G_2(I = 3/2)/G_2(I = 2)$. The nuclear g factor was set to $g = 0.35$ and the nuclear lifetime varied. The thick black line represents the model parameters that best fit the RIV data for Te ions in Ref. [13]. The other lines examine sensitivity to the average atomic spin and the rate and duration of atomic transitions.

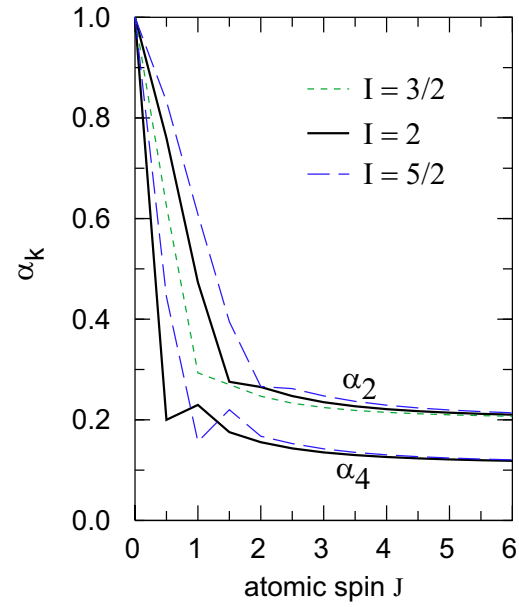

FIG. 8. Atomic spin (J) dependence of the hard-core vacuum attenuation coefficients for nuclear spins $I = 3/2, 2, 5/2$.

discuss the impact of the parametrization of G_k as a function of $g^2\tau$ rather than as a function of $g\tau$. Third, we assess the influence of the value of the hard core of the attenuation coefficient on the extracted g factor. Fourth, we examine the effect of the small differences in the velocity with which ions of the different Te isotopes emerge into vacuum. Finally we discuss progress toward *ab initio* atomic structure calculations that might ultimately make empirical calibrations of the RIV interaction unnecessary.

A. Nuclear spin dependence of G_k

Figure 7 shows toy model Monte Carlo calculations of $G_k(I = 3/2)/G_k(I = 2)$ and $G_k(I = 5/2)/G_k(I = 2)$ as a function of the nuclear mean life. The nuclear g factor was set to $g = 0.35$ and the nuclear lifetime varied. The black line, which represents the model parameters that best fit the RIV data for Te ions in Ref. [13], shows very little deviation from unity. The other lines explore the consequences of varying the average atomic spin and the rate and number of atomic transitions. The most extreme case (for which the individual G_k values do not fit the experimental data) has a reduced average atomic spin and very few nuclear transitions. As a rule, the variation of the attenuation coefficients for nuclear spins $I = 2 \pm \frac{1}{2}$ is small when the average atomic spin increases and/or if there are an increased number of atomic transitions.

These calculations make it clear that, to the precision of the present data, the G_k values for the $3/2^+$ and $5/2^+$ states in ^{125}Te can be compared directly with those measured for the 2^+ states of the even isotopes. Further insights into this equivalence can be gained from Fig. 8, which indicates that the hard core values for the alternative nuclear spins converge once the atomic spin exceeds $J = 2$.

B. Parametrization of G_k: $g^2\tau$ versus $g\tau$

If the data for the $5/2^+$ level of ^{125}Te are ignored (not a justified procedure, particularly as consistent G_k values are extracted from both the 463-keV $E2$ transition and the mixed multipolarity $M1/E2$ 428-keV transition), then the G_k data can be parametrized quite well as a function of $g\tau$, as indicated in Fig. 9, which shows the results for BareBall ring 3. The ^{136}Te g factor extracted based on this parametrization is then $g = 0.28^{+0.10}_{-0.06}$. (The uncertainty in the lifetime is not

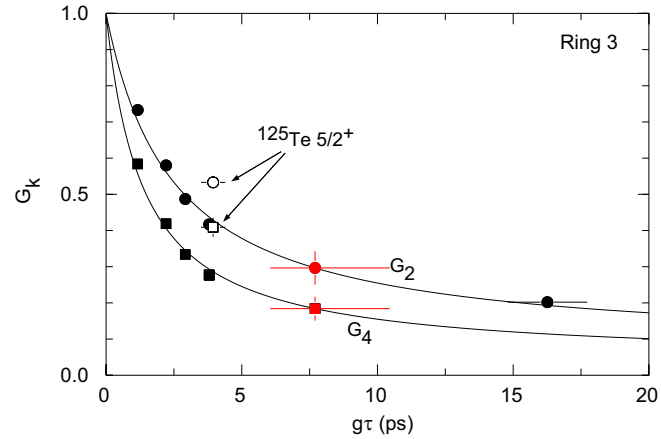

FIG. 9. G_k versus $g\tau$ calibration curves for BareBall ring 3 ignoring data for the $5/2^+$ state in ^{125}Te. The best fit $g\tau$ value for ^{136}Te, and its uncertainty, is projected onto the curves (red filled). See also Fig. 6.

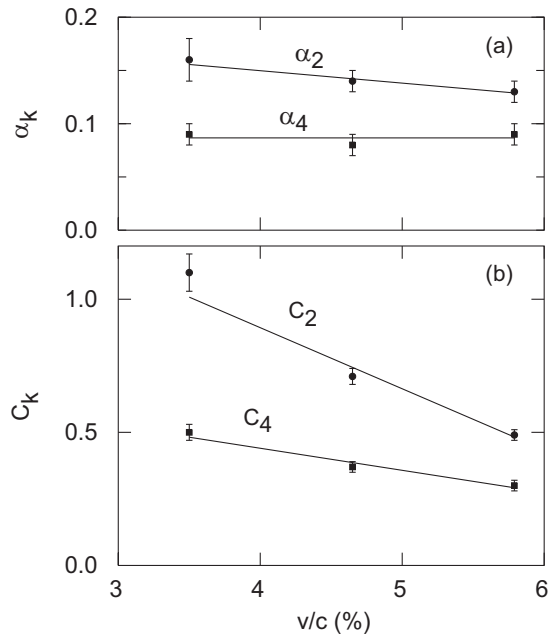

FIG. 10. Dependence of the parameters (a) α_k and (b) C_k, Eqs. (10) and (11), on ion velocity. Lines indicate linear fits.

included.) This value should be compared to $g = 0.34^{+0.07}_{-0.06}$ from the equivalent analysis assuming G_k is a function of $g^2\tau$. The two values overlap within uncertainties.

C. Influence of hard core on *g* factor

If the data for the $3/2^+$ level of ^{125}Te are ignored, the hard core value is not well defined experimentally and indeed fits to the remaining data favor $\alpha_2 = \alpha_4 = 0$. Although this is evidently unphysical, its impact on the extracted g factor was investigated, yielding $g = 0.29 \pm 0.03$ for the case where G_k is parametrized as a function of $g^2\tau$. It is evident that as the hard-core value increases, the extracted g factor increases, as does its uncertainty, which becomes asymmetric.

Here, as in the preceding subsection, where alternative, arguably unphysical, analysis procedures are used, the extracted g factor remains near $g = 0.3$, which is a typical value for heavy collective nuclei. It can be concluded that the uncertainties in the RIV calibration are small compared with the statistical uncertainty.

D. Velocity dependence of the RIV interaction

As evident in Table I, despite efforts to match the kinematic conditions by adjusting the beam energy, the different Te isotopes emerge from the target into vacuum with slightly different average velocities. These differences in velocity are small compared to the differences in velocity from ring to ring of BareBall. The effect of the small variations with isotope can be assessed by examining the variation of the parameters of the hyperfine interaction calibration, Eqs. (10) and (11), as a function of ion velocity, as shown in Fig. 10. The hard core values, α_k, are insensitive to the ion velocity, whereas the C_k values decrease with increasing velocity, approximately linearly. Noting that the extracted value of g^2 scales with C_k, and taking the range of variation in v/c with isotope from Table I, together with the slope of the line that describes C_2 versus v/c in Fig. 10, it can be shown that the error on the extracted g factor associated with ignoring the variation in velocity across the range of isotopes is below the level of 0.5%. This error is negligible compared to other sources of uncertainty.

E. Status of *ab initio* RIV calculations

With the computer power available today, along with comprehensive atomic structure codes such as the multiconfiguration Hartree-Fock (MCHF) atomic structure package [15], [19] and GRASP2K [20], it has become reasonable to attempt *ab initio* calculations of the free-ion hyperfine interactions of relevance to RIV and magnetic moment measurements.

The simplest microscopic approach to model the RIV attenuation for many electron ions is to superimpose the deorientation coefficients for the calculated hyperfine interactions up to a cut-off in excitation energy, assuming a weighting factor of $(2J + 1)$ for each atomic state. Stone *et al.* [39] have reported such calculations for Mo, Ru, and Pd ions recoiling into vacuum with velocity $v/c \sim 0.05$, and more recently for ^{54,56}Fe ions at $v/c \sim 0.08$ [40]. This static model can then be improved by including the effect of atomic transitions, based on the calculated atomic level lifetimes, which Stone *et al.* also explored [39,40]. Chen *et al.* [21] have taken the calculations further by implementing a Monte Carlo method to evaluate the effect of atomic transitions and applying it to the tellurium isotopes. In their work, rather than an energy cut-off, the maximum number of electrons excited from the ground-state configuration is treated as a free parameter.

The most important outcome of the work of Chen *et al.* for the present work on the Te isotopes is the recognition, based on atomic calculations, that many electronic states have lifetimes comparable to or shorter than the nuclear lifetime and that atomic transitions may therefore contribute strongly to the observed average hyperfine interaction. Indeed the empirical modeling of the hyperfine interactions for Te ions recoiling into vacuum with $v/c \sim 0.06$ reported in Ref. [13] indicated that there is evidence for several atomic transitions taking place on the time-scale of ~10 ps (see Fig. 7 of [13]).

The main limitation that makes first-principles calculations impractical at present is that the initial population of atomic states, when the ion enters vacuum, is not well known. For example, the calculations described above do not describe atomic structure effects that are seen in otherwise similar measurements of free-ion hyperfine interactions for Ge and Se ions carrying ~12–15 electrons, as reported in Ref. [35]. The difference in the G_k versus $g\tau$ dependence is prominent in the hard-core region, and apparently stems from a difference in the average atomic angular momentum in the range between $\bar{J} = 1$ and $\bar{J} = 2$ for Ge versus Se ions within about 10 ps of the ions entering vacuum. This observation implies that there is a strong preference to populate lower-excited atomic states soon after the ions enter vacuum and that for these ions $\bar{J}$ is rather sensitive to the charge state of the ion. As

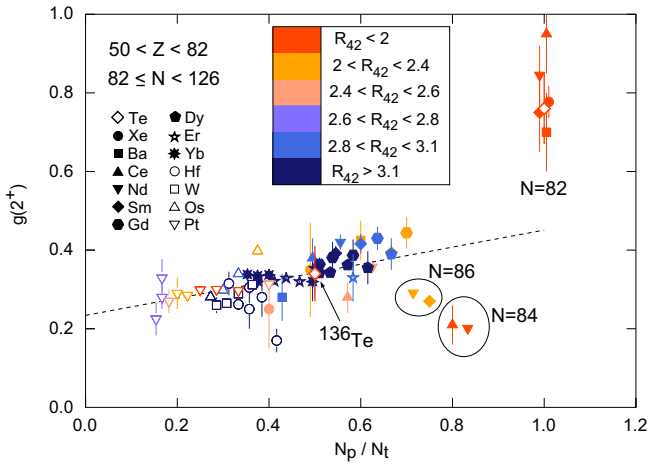

FIG. 11. First-excited 2^+ state g factors as a function of the valence proton fraction, N_p/N_t, for nuclei with $50 < Z < 82$ and $82 \leqslant N < 126$. The broken line indicates the trend for $N_p/N_t < 0.7$. Data points (from Refs. [14,41] and present work) are colored (shaded) to indicate $R_{42} = E_x(4_1^+)/E_x(2_1^+)$. Note that only the $N = 82$ and $N = 84$ isotones have $R_{42} < 2$.

evident in Fig. 8, the hard core attenuation coefficients vary somewhat with atomic spin for $J < 2$ but become insensitive to J for $J \geqslant 2$. The discontinuous behavior of the Ge and Se ions carrying ~12–15 electrons gives insight into the RIV atomic interactions, and more detailed atomic calculations are in progress. Fortunately similar effects are not expected in the present work. The Te ions enter vacuum typically carrying ~22–32 electrons, with the majority of ions for BareBall rings 3 and 4 carrying ~22–27 electrons. The low-excitation atomic states of these ions are dominated by relatively high spin ($J \sim 4$) $3d^n$ configurations, which together with Fig. 8 then suggests that the RIV interaction will be less sensitive to the charge states of such ions.

Thus although there has been considerable progress, the point has not yet been reached whereby *ab initio* atomic calculations can reliably calculate the RIV hyperfine interaction for complex many-electron ions. Experimental data on similar atomic systems for isotopes with known g factors are still needed to define the hyperfine interaction, and, in essence, the calibration procedures remain empirical.

V. NUCLEAR STRUCTURE AND THE g FACTOR OF ^{136}Te

A. g-factor systematics in the major shell

Figure 11 shows the g factors of the first 2^+ states in the major shell with $50 < Z < 82$ and $82 \leqslant N < 126$ plotted as a function of the valence proton fraction. The g factor of ^{136}Te with two valence protons and two valence neutrons outside ^{132}Sn is in excellent agreement with the g factors of other nuclei with equal numbers of valence protons and neutrons (or proton holes and neutron holes) in the major shell. For these nuclei $N_n = N_p$ and $N_t = N_p + N_n$ so $N_p/N_t = 0.5$, where $N_p(N_n)$ is the number of valence protons (neutrons) and N_t is the total number of valence nucleons. Besides ^{136}Te the other nuclides with $N_p/N_t = 0.5$ are ^{140}Xe, ^{144}Ba, ^{148}Ce, ^{160}Gd, ^{164}Dy, and ^{164}Er.

The g factor of ^{136}Te, however, is not in agreement with the g factors of the other $N = 84$ isotones ^{142}Ce and ^{144}Nd. A reduced g factor, well below Z/A, when two neutrons are added outside $N = 52$ has been observed for ^{90}Sr [42], ^{92}Zr [43], and ^{94}Mo [44]. In these cases the added neutrons occupy mainly the $\nu d_{5/2}$ orbit. Several theoretical calculations [2,3,18] anticipated similar behavior for ^{136}Te, which is not observed. The change in the behavior of the g factors, which decrease along $N = 84$ from ^{136}Te to ^{144}Nd, can be related to differences in the relative excitations of the 2^+ excitations in the proton and neutron subsystems, and to the strength of the coupling between them [44–46]. Particle-core coupling model calculations by Copnell *et al.* [47] predicted decreasing g factors from ^{138}Xe to ^{144}Nd, which track with a decreasing particle-core (i.e., neutron-proton) coupling strength along the sequence. The $N = 86$ isotones with measured g factors, namely ^{140}Xe [48], ^{142}Ba [49], ^{146}Nd [50], and ^{148}Sm [51,52], show a similar but possibly less-pronounced trend. The fact that the proton Fermi surface is moving through the $\pi g_{7/2}$ subshell into the $\pi d_{5/2}$ subshell and toward the $Z = 64$ subshell closure, while the neutrons remain mainly in the $\nu f_{7/2}$ orbit, might play a role in changing the proton-neutron balance. Additional model calculations and experimental g factors for ^{138}Xe and ^{140}Ba would be of value to illuminate this unexpected behavior.

B. Shell model calculations and electromagnetic properties around ^{132}Sn

Shell model calculations were performed with the NUSHELLX@MSU code [53] for the Te and Xe isotopes with two and four neutrons or neutron holes relative to ^{132}Sn. All proton single-particle orbits in the $Z = 50$–82 shell ($\pi 1g_{7/2}, 2d_{5/2}, 2d_{3/2}, 3s_{1/2}, 1h_{11/2}$) were included. For the cases with $N < 82$ all neutron orbits in the $N = 50$–82 shell ($\nu 1g_{7/2}, 3d_{5/2}, 3d_{3/2}, 3s_{1/2}, 1h_{11/2}$) and for $N > 82$ all neutron orbits in the $N = 82$–126 shell ($\nu 1h_{9/2}, 2f_{7/2}, 2f_{5/2}, 3p_{3/2}, 3p_{1/2}, 1i_{13/2}$) were included. Single particle energies were set by reference to the low-excitation spectra of ^{133}Sb and ^{133}Sn for protons and neutrons, respectively, and ^{131}Sn for neutron holes. As described in Refs. [4,18,54], the interactions were based on the CD Bonn potential with the renormalization of the G matrix carried to third order, and a Coulomb term added to the proton-proton interaction. The effective charges were $e_p = 1.5e$ and $e_n = 0.5e$. The effect of raising the neutron effective charge to $e_n = 0.8e$ for $N < 82$ was also explored.

The effective $M1$ operator applied a correction $\delta g_l(p) = 0.13$ to the proton orbital g factor and quenched the spin g factors for both protons and neutrons to 70% of their bare values. (The tensor term was ignored.) The effective $M1$ operator is then similar to that of Jakob *et al.* [1] and in reasonable agreement with that of Brown *et al.* [4]. Table IV compares the experimental g factors [41] of some 'simple' states near ^{132}Sn with theoretical g factors evaluated with the bare and effective $M1$ operators. The effective operator is essential to describe states with a dominant $\pi g_{7/2}$ configuration. Fortunately it

TABLE IV. g factors of few-nucleon states near ^{132}Sn.

Nuclide	J^π	Main configuration	g factor		
			Bare	SM	Exp [41]
^{133}Sb	$7/2^+_1$	$\pi g_{7/2}$	+0.491	+0.821	+0.857(3)
^{134}Te	2^+_1	$\pi(g_{7/2})^2$	+0.514	+0.836	+0.76(9)
	4^+_1		+0.509	+0.832	$+0.70^{+0.55}_{-0.38}$
	6^+_1		+0.514	+0.842	+0.847(25)
^{135}I	$7/2^+_1$	$\pi(g_{7/2})^3$	+0.492	+0.822	+0.840(1)
^{135}Te	$7/2^-_1$	$\pi(g_{7/2})^2_0 \otimes \nu f_{7/2}$	−0.238	−0.272	−0.197(14)
^{137}Xe	$7/2^-_1$	$\pi(g_{7/2})^4_0 \otimes \nu f_{7/2}$	−0.240	−0.251	−0.277(2)

is less important for $\nu f_{7/2}$ configurations, for which there is little experimental data, and moreover there is also a discrepancy between the experimental $7/2^-$ ground-state moments of ^{135}Te and ^{137}Xe, which are expected to have similar values.

The g factors and $B(E2; 2^+_1 \rightarrow 0^+_1)$ values for the Te and Xe isotopes between $N = 78$ and $N = 84$ are compared with experiment [1,7,12,14,18,27,48,55–57] in Fig. 12. Overall the description of these electromagnetic observables is very good, especially for the limited data available for $N \geqslant 82$. The description of the $B(E2)$ values is improved for $N < 82$ by increasing the neutron effective charge to $e_n = 0.8$, although there remains some shortfall in $E2$ strength. Most recent theoretical work has focused on the neutron-rich isotopes beyond $N = 82$ where an anomalously low $B(E2)$ was observed in ^{136}Te [11]. The new $B(E2)$ data are seen to agree well with expectations, and the shell model calculations also describe the g factors and energy levels well (see Refs. [4,54]). In all, the results affirm the evidence from mass measurements and neutron-separation energies

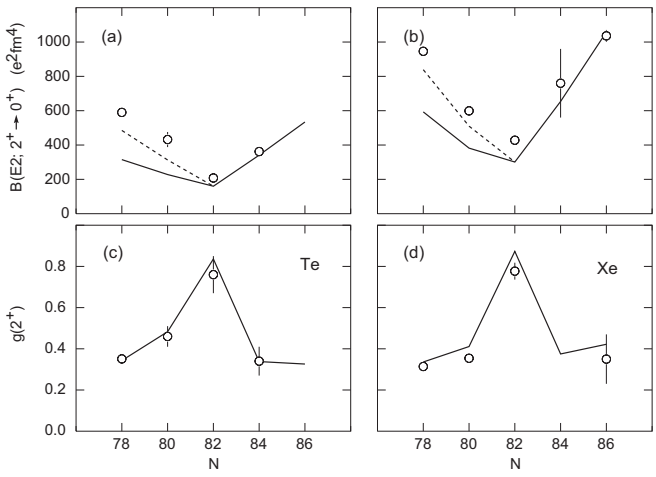

FIG. 12. Reduced transition rates and g factors of Te and Xe isotopes spanning $N = 82$. The dotted lines in (a) and (b) correspond to an increased neutron effective charge of $e_n = 0.8$ for $N < 82$. Experimental data from Refs. [1,7,12,14,18,27,48,55–57].

[58–61], decay spectroscopy [62–66], Coulomb excitation [14,15,17,67,68], and transfer reactions [69,70], that ^{132}Sn is a good doubly magic nucleus. They furthermore indicate that the nucleon-nucleon interactions based on a G matrix derived from the CD Bonn potential with renormalization carried to third order [4] are appropriate for neutron-rich nuclei near ^{132}Sn.

VI. SUMMARY AND CONCLUSIONS

The g factor of the first-excited state of ^{136}Te with two proton and two neutrons outside of the ^{132}Sn double shell closure has been measured by the recoil in vacuum method, following Coulomb excitation of the radioactive ^{136}Te beam. A detailed description of the analysis procedures has been given. The approximations employed in the analysis have been described and assessed, demonstrating a robust resultant g factor.

The experimental g factor fits well with systematics of other nuclei with equal numbers of valence protons and neutrons in the $50 \leqslant Z \leqslant 82$ and $82 \leqslant N \leqslant 126$ major shell but an unexpected trend in $g(2^+_1)$ for the $N = 84$ isotones, which decrease from ^{136}Te to ^{144}Nd, is exposed.

Shell model calculations with interactions derived from the CD Bonn potential show good agreement with the g factors and $E2$ transition rates of 2^+ states around ^{132}Sn, confirming earlier indications that ^{132}Sn is a good doubly magic core.

The methodology described here could be applied for similar simultaneous measurements of $B(E2)$, $Q(2^+)$, and $g(2^+)$ in other regions of the nuclear chart. For example, applications to few-nucleon 2^+ states around ^{208}Pb would be of considerable interest. The shell structure in the neutron-rich ^{132}Sn region can be compared with that in the vicinity of stable ^{208}Pb [71,72]. While the high-spin structure has been quite thoroughly studied experimentally around ^{208}Pb, the electromagnetic properties of low-excitation, low-spin states associated with a few pairs of valence nucleons outside ^{208}Pb have not. Thus direct comparisons of the related few-particle states around ^{132}Sn and ^{208}Pb are currently limited by the lack of experimental data on electromagnetic properties near ^{208}Pb rather than near ^{132}Sn. Measurements of the type proposed here on ^{210}Pb, ^{210}Po, and ^{212}Po would enable comparison with their equivalents, ^{134}Sn, ^{134}Te, and ^{136}Te.

ACKNOWLEDGMENTS

The authors gratefully acknowledge the HRIBF operations staff for providing the beams used in this study. This material is based upon work supported by the U.S. Department of Energy, Office of Science, Office of Nuclear Physics, under Contract No. DE-AC05-00OR22725, and this research used resources of the Holifield Radioactive Ion Beam Facility of Oak Ridge National Laboratory, which was a DOE Office of Science User Facility. This research was also sponsored by the Australian Research Council under Grant No. DP0773273 and by the U.S. DOE under Contract No. DE-FG02-96ER40963 (UTK).

[1] G. Jakob, N. Benczer-Koller, G. Kumbartzki, J. Holden, T. J. Mertzimekis, K.-H. Speidel, R. Ernst, A. E. Stuchbery, A. Pakou, P. Maier-Komor *et al.*, Phys. Rev. C **65**, 024316 (2002).

[2] J. Terasaki, J. Engel, W. Nazarewicz, and M. Stoitsov, Phys. Rev. C **66**, 054313 (2002).

[3] N. Shimizu, T. Otsuka, T. Mizusaki, and M. Honma, Phys. Rev. C **70**, 054313 (2004).

[4] B. A. Brown, N. J. Stone, J. R. Stone, I. S. Towner, and M. Hjorth-Jensen, Phys. Rev. C **71**, 044317 (2005).

[5] A. Covello, L. Coraggio, A. Gargano, and N. Itaco, Prog. Part. Nucl. Phys. **59**, 401 (2007).

[6] L. Coraggio, A. Covello, A. Gargano, N. Itaco, and T. Kuo, Prog. Part. Nucl. Phys. **62**, 135 (2009).

[7] M. Danchev, G. Rainovski, N. Pietralla, A. Gargano, A. Covello, C. Baktash, J. R. Beene, C. R. Bingham, A. Galindo-Uribarri, K. A. Gladnishki *et al.*, Phys. Rev. C **84**, 061306(R) (2011).

[8] S. M. Wang, J. C. Pei, and F. R. Xu, Phys. Rev. C **87**, 014311 (2013).

[9] D. Bianco, N. Lo Iudice, F. Andreozzi, A. Porrino, and F. Knapp, Phys. Rev. C **88**, 024303 (2013).

[10] A. P. Severyukhin, N. N. Arsenyev, N. Pietralla, and V. Werner, Phys. Rev. C **90**, 011306(R) (2014).

[11] D. C. Radford, C. Baktash, J. R. Beene, B. Fuentes, A. Galindo-Uribarri, C. J. Gross, P. A. Hausladen, T. A. Lewis, P. E. Mueller, E. Padilla *et al.*, Phys. Rev. Lett. **88**, 222501 (2002).

[12] N. J. Stone, A. E. Stuchbery, M. Danchev, J. Pavan, C. L. Timlin, C. Baktash, C. Barton, J. Beene, N. Benczer-Koller, C. R. Bingham *et al.*, Phys. Rev. Lett. **94**, 192501 (2005).

[13] A. E. Stuchbery and N. J. Stone, Phys. Rev. C **76**, 034307 (2007).

[14] A. E. Stuchbery, J. M. Allmond, A. Galindo-Uribarri, E. Padilla-Rodal, D. C. Radford, N. J. Stone, J. C. Batchelder, J. R. Beene, N. Benczer-Koller, C. R. Bingham *et al.*, Phys. Rev. C **88**, 051304(R) (2013).

[15] J. M. Allmond, A. E. Stuchbery, D. C. Radford, A. Galindo-Uribarri, N. J. Stone, C. Baktash, J. C. Batchelder, C. R. Bingham, M. Danchev, C. J. Gross *et al.*, Phys. Rev. C **87**, 054325 (2013).

[16] J. M. Allmond, A. E. Stuchbery, A. Galindo-Uribarri, E. Padilla-Rodal, D. C. Radford, J. C. Batchelder, C. R. Bingham, M. E. Howard, J. F. Liang, B. Manning *et al.*, Phys. Rev. C **92**, 041303(R) (2015).

[17] J. M. Allmond, D. C. Radford, C. Baktash, J. C. Batchelder, A. Galindo-Uribarri, C. J. Gross, P. A. Hausladen, K. Lagergren, Y. Larochelle, E. Padilla-Rodal *et al.*, Phys. Rev. C **84**, 061303(R) (2011).

[18] J. M. Allmond, A. E. Stuchbery, C. Baktash, A. Gargano, A. Galindo-Uribarri, D. C. Radford, C. R. Bingham, B. A. Brown, L. Coraggio, A. Covello *et al.*, Phys. Rev. Lett. **118**, 092503 (2017).

[19] N. Benczer-Koller, G. J. Kumbartzki, G. Gürdal, C. J. Gross, A. E. Stuchbery, B. Krieger, R. Hatarik, P. O'Malley, S. Pain, L. Segen *et al.*, Phys. Lett. B **664**, 241 (2008).

[20] G. J. Kumbartzki, N. Benczer-Koller, D. A. Torres, B. Manning, P. D. O'Malley, Y. Y. Sharon, L. Zamick, C. J. Gross, D. C. Radford, S. J. Q. Robinson *et al.*, Phys. Rev. C **86**, 034319 (2012).

[21] X. Chen, D. G. Sarantites, W. Reviol, and J. Snyder, Phys. Rev. C **87**, 044305 (2013).

[22] A. E. Stuchbery and M. P. Robinson, Nuclear Instrum. Methods Phys. Res. A **485**, 753 (2002).

[23] A. E. Stuchbery, Nucl. Phys. A **723**, 69 (2003).

[24] K. Alder and A. Winther, *Electromagnetic Excitation* (North-Holland, Amsterdam, 1975).

[25] C. J. Gross, T. N. Ginter, D. Shapira, W. T. Milner, J. W. McConnell, A. N. James, J. W. Johnson, J. Mas, P. F. Mantica, R. L. Auble *et al.*, Nuclear Instrum. Methods Phys. Res. A **450**, 12 (2000).

[26] A. Galindo-Uribarri, AIP Conf. Proc. **1271**, 180 (2010).

[27] A. E. Stuchbery, A. Nakamura, A. N. Wilson, P. M. Davidson, H. Watanabe, and A. I. Levon, Phys. Rev. C **76**, 034306 (2007).

[28] S. K. Chamoli, A. E. Stuchbery, and M. C. East, Phys. Rev. C **80**, 054301 (2009).

[29] N. Benczer-Koller, G. Lenner, R. Tanczyn, A. Pakou, G. Kumbartzki, A. Piqué, D. Barker, D. Berdichevsky, and L. Zamick, Phys. Rev. C **40**, 77 (1989).

[30] T. Tamura, Nucl. Data Sheets **108**, 455 (2007).

[31] J. Katakura and Z. Wu, Nucl. Data Sheets **109**, 1655 (2008).

[32] J. Katakura, Nucl. Data Sheets **112**, 495 (2011).

[33] J. Katakura and K. Kitao, Nucl. Data Sheets **97**, 765 (2002).

[34] B. Singh, Nucl. Data Sheets **93**, 33 (2001).

[35] A. E. Stuchbery, Hyperfine Interact. **220**, 29 (2013).

[36] A. Abragam and R. V. Pound, Phys. Rev. **92**, 943 (1953).

[37] I. B. Zvi, P. Gilad, M. Goldberg, G. Goldring, A. Schwarzschild, A. Sprinzak, and Z. Vager, Nucl. Phys. A **121**, 592 (1968).

[38] R. Brenn, H. Spehl, A. Weckherlin, H. A. Doubt, and G. van Middelkoop, Z. Phys. A **281**, 219 (1977).

[39] N. J. Stone, J. R. Stone, and P. Jonsson, Hyperfine Interact. **197**, 29 (2010).

[40] N. J. Stone, J. R. Stone, A. E. Stuchbery, and P. Jonsson, Hyperfine Interact. **230**, 169 (2015).

[41] N. J. Stone, INDC(NDS)-0658 (2014), https://www-nds.iaea.org/publications/indc/indc-nds-0658/.

[42] G. J. Kumbartzki, N. Benczer-Koller, S. Burcher, A. Ratkiewicz, S. L. Rice, Y. Y. Sharon, L. Zamick, K.-H. Speidel, D. A. Torres, K. Sieja *et al.*, Phys. Rev. C **89**, 064305 (2014).

[43] G. Jakob, N. Benczer-Koller, J. Holden, G. Kumbartzki, T. J. Mertzimekis, K. H. Speidel, C. W. Beausang, and R. Krücken, Phys. Lett. B **468**, 13 (1999).

[44] P. F. Mantica, A. E. Stuchbery, D. E. Groh, J. I. Prisciandaro, and M. P. Robinson, Phys. Rev. C **63**, 034312 (2001).

[45] A. E. Stuchbery, Nucl. Phys. A **682**, 470 (2001).

[46] A. E. Stuchbery, J. Phys.: Conf. Ser. **387**, 012012 (2012).

[47] J. Copnell, S. J. Robinson, J. Jolie, and K. Heyde, Phys. Rev. C **46**, 1301 (1992).

[48] C. Goodin, J. R. Stone, N. J. Stone, A. V. Ramayya, A. V. Daniel, J. H. Hamilton, K. Li, J. K. Hwang, G. M. Ter-Akopian, and J. O. Rasmussen, Phys. Rev. C **79**, 034316 (2009).

[49] A. Wolf, R. L. Gill, H. Mach, R. F. Casten, and J. A. Winger, Phys. Rev. C **37**, 1253 (1988).

[50] J. Holden, N. Benczer-Koller, G. Jakob, G. Kumbartzki, T. J. Mertzimekis, K.-H. Speidel, C. W. Beausang, R. Krücken, A. Macchiavelli, M. McMahan *et al.*, Phys. Rev. C **63**, 024315 (2001).

[51] D. Bazzacco, F. Brandolini, K. Löwenich, P. Pavan, and C. Rossi-Alvarez, Z. Phys. A **328**, 275 (1987).

[52] N. Benczer-Koller, D. J. Ballon, and A. Pakou, Hyperfine Interact. **33**, 37 (1987).

[53] B. A. Brown, W. D. M. Rae, E. McDonald, and M. Horoi, NUSHELLX@MSU, https://people.nscl.msu.edu/~brown/resources/resources.html.

[54] J. M. Allmond, A. E. Stuchbery, B. A. Brown, J. R. Beene, A. Galindo-Uribarri, C. J. Gross, J. F. Liang, E. Padilla-Rodal, D. C. Radford, R. L. Varner *et al.*, Phys. Rev. C **90**, 014322 (2014).
[55] S. Raman, C. W. Nestor, and P. Tikkanen, At. Data Nucl. Data Tables **78**, 1 (2001).
[56] T. Kröll, T. Behrens, R. Krücken, V. Bildstein, R. Gernhäuser, P. Maierbeck, I. Stefanescu, O. Ivanov, J. Van de Walle, N. Warr *et al.*, Euro. Phys. J. Special Topics **150**, 127 (2007).
[57] A. Lindroth, B. Fogelberg, H. Mach, M. Sanchez-Vega, and J. Bielčík, Phys. Rev. Lett. **82**, 4783 (1999).
[58] B. Fogelberg, K. A. Mezilev, H. Mach, V. I. Isakov, and J. Slivova, Phys. Rev. Lett. **82**, 1823 (1999).
[59] M. Dworschak, G. Audi, K. Blaum, P. Delahaye, S. George, U. Hager, F. Herfurth, A. Herlert, A. Kellerbauer, H.-J. Kluge *et al.*, Phys. Rev. Lett. **100**, 072501 (2008).
[60] J. Hakala, J. Dobaczewski, D. Gorelov, T. Eronen, A. Jokinen, A. Kankainen, V. S. Kolhinen, M. Kortelainen, I. D. Moore, H. Penttilä *et al.*, Phys. Rev. Lett. **109**, 032501 (2012).
[61] J. Van Schelt, D. Lascar, G. Savard, J. A. Clark, P. F. Bertone, S. Caldwell, A. Chaudhuri, A. F. Levand, G. Li, G. E. Morgan *et al.*, Phys. Rev. Lett. **111**, 061102 (2013).
[62] A. Kerek, G. B. Holm, L.-E. De Geer, and S. Borg, Phys. Lett. B **44**, 252 (1973).
[63] T. Björnstad, L.-E. De Geer, G. T. Ewan, P. G. Hansen, B. Jonson, K. Kawade, A. Kerek, W.-D. Lauppe, H. Lawin, S. Mattsson *et al.*, Phys. Lett. B **91**, 35 (1980).
[64] K. Kawade, K. Sistemich, G. Battistuzzi, H. Lawin, K. Shizuma, and J. Blomqvist, Z. Phys. A **308**, 33 (1982).
[65] B. Fogelberg, M. Hellström, D. Jerrestam, H. Mach, J. Blomqvist, A. Kerek, L. O. Norlin, and J. P. Omtvedt, Phys. Rev. Lett. **73**, 2413 (1994).
[66] P. Bhattacharyya, P. J. Daly, C. T. Zhang, Z. W. Grabowski, S. K. Saha, R. Broda, B. Fornal, I. Ahmad, D. Seweryniak, I. Wiedenhöver *et al.*, Phys. Rev. Lett. **87**, 062502 (2001).
[67] J. Beene, R. Varner, C. Baktash, A. Galindo-Uribarri, C. Gross, J. G. del Campo, M. Halbert, P. Hausladen, Y. Larochelle, J. Liang *et al.*, Nucl. Phys. A **746**, 471 (2004).
[68] D. C. Radford, C. Baktash, C. J. Barton, J. Batchelder, J. R. Beene, C. R. Bingham, M. A. Caprio, M. Danchev, B. Fuentes, A. Galindo-Uribarri *et al.*, Nucl. Phys. A **752**, 264 (2005).
[69] K. L. Jones, A. S. Adekola, D. W. Bardayan, J. C. Blackmon, K. Y. Chae, K. A. Chipps, J. A. Cizewski, L. Erikson, C. Harlin, R. Hatarik *et al.*, Nature **465**, 454 (2010).
[70] J. M. Allmond, A. E. Stuchbery, J. R. Beene, A. Galindo-Uribarri, J. F. Liang, E. Padilla-Rodal, D. C. Radford, R. L. Varner, A. Ayres, J. C. Batchelder *et al.*, Phys. Rev. Lett. **112**, 172701 (2014).
[71] L. Coraggio, A. Covello, A. Gargano, and N. Itaco, Phys. Rev. C **80**, 021305(R) (2009).
[72] A. Gargano, L. Coraggio, A. Covello, and N. Itaco, J. Phys.: Conf. Ser. **168**, 012013 (2009).